Supporting Information

Acid-Mediated Modulation of the Conductance of Diazapentalene Molecular Junctions

Jianming An,[1] Xiaoqi Luo,[2] Sumit Naskar,[3] Di Wu,*[2] Carmen Herrmann,[3] Jianlong Xia,*[2] Haixing Li,*[1]

[1]Department of Physics, City University of Hong Kong, Kowloon 999077, Hong Kong, China
[2]International School of Materials Science and Engineering, Wuhan University of Technology, Wuhan 430070, China; State Key Laboratory of Advanced Technology for Materials Synthesis and Processing, Center of Smart Materials and Devices and School of Chemistry, Chemical Engineering and Life Science, Wuhan University of Technology, Wuhan 430070, China
[3]Department of Chemistry, University of Hamburg, Harbor Bldg. 610, Luruper Chaussee 149, 22761 Hamburg, Germany; The Hamburg Centre for Ultrafast Imaging, University of Hamburg, Luruper Chaussee 149, 22761 Hamburg, Germany

Jianming An and Xiaoqi Luo contributed equally to this work

Table of Contents

I. Synthetic Procedures and Characterization of Compounds

All chemical reactions were conducted in oven-dried or flame-dried glassware. All the chemicals and starting materials were purchased from commercial sources without further treatment unless specially noted. Anhydrous toluene was dried over sodium shavings. The compound **2**[1] and **3**[2] were synthesized according to the published procedures.

^{1}H NMR and ^{13}C NMR spectra were measured on Bruker Avance III HD. MALDI-TOF Mass spectrum was measured with AB Sciex 5800. UV-vis spectrum was recorded on Shimadzu UV-1800. Cyclic voltammograms (CVs) were obtained on CHI660E electrochemical workstation. A three-electrode one-compartment cell containing a solution of the analyte and supporting electrolyte (tetrabutylammonium, ($[NBu_4]PF_6$), 0.1 M) in dry CH_2Cl_2 was utilized. The three-electrode system include a 500 μm diameter platinum-disk as working electrode, a platinum-wire as counter electrode, and an Ag/AgCl as reference electrode. The measurements were obtained under a scanning rate of 100 mV/s.

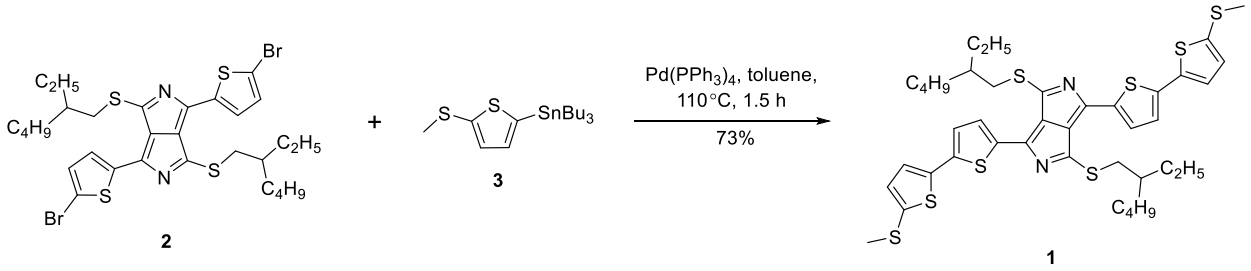

Compound **1**: In a 100 mL two-neck round bottom flask under ambient atmosphere, compound **3** (147 mg, 0.35 mmol) and **2** (100 mg, 0.14 mmol) were added. The flash was purged with N_2 for 20 min, followed by the addition of $Pd(PPh_3)_4$ (16 mg, 0.014 mmol) and toluene (50 mL). The resulting mixture was refluxed for 1.5 h. After this mixture was cooled down to room temperature, water was added and the resulting mixture was extracted with CH_2Cl_2 three times, the organic mixture was washed with brine, and dried over Na_2SO_4. After evaporation of the solvent, the residue was purified on a silica-gel column chromatography with CH_2Cl_2 : PE = 1 : 1. Compound **1** (83 mg, 73%) was obtained as a blue solid. ^{1}H NMR (500 MHz, Chloroform-d) δ 7.99 (d, J = 4.0 Hz, 2H), 7.28 (d, J = 4.0 Hz, 2H), 7.18 (d, J = 3.6 Hz, 2H), 6.99 (d, J = 3.6 Hz, 2H), 3.58 (dd, J = 13.1, 5.7 Hz, 2H), 3.48 (dd, J = 13.1, 6.6 Hz, 2H), 2.55 (s, 6H), 1.83 (s, 2H), 1.46 (s, 16H), 0.94 (s, 12H). ^{13}C NMR (126 MHz, Chloroform-d) δ 165.6, 150.7, 143.5, 139.0, 138.8, 138.1, 133.5, 132.1, 131.2, 125.5, 125.3, 77.3, 77.0, 76.8, 39.8, 36.5, 32.8, 29.1, 25.9, 23.1, 21.6, 14.2, 11.1, 0.0. MS (MALDI-TOF) m/z: [M]+ Calculated for $C_{40}H_{48}N_2S_8$ 812.16; Found 812.41.

II. Scanning Tunneling Microscope Break-Junction Experiment Details

All single molecule junction conductance measurements were performed using a custom-built STM-BJ setup that was controlled by a custom software (IgorPro, Wavemetrics, Inc.)

and operated in ambient conditions at room temperature (details provided previously[3]). We prepared a molecular solution of 0.1 mM **1** in TCB, and we additionally added 0.3 ~ 0.6 μL TFA into a ~ 1 mL molecular solution in TCB for preparing the solution with molar ratio of 1 : 40, 1 : 80, and 1 : 200 between **1** and TFA. We applied ultrasonic mixing to the solution for 10 minutes before each conductance experiment. We used a 0.25 mm diameter gold wire (99.999%, Hebei Hongju Metal Materials Co. Ltd) and a steel surface coated with ~ 150 nm gold film prepared using a sputtering machine as the STM tip and substrate respectively. 1,2,4-trichlorobenzene was purchased from Aladdin (anhydrous, ≥ 99%). Trifluoroacetic acid was purchased from Aladdin (standard for GC, ≥ 99.5%). For all measurements, we used 40 kHz data acquisition rate and a speed of 30 nm/s for withdrawing the tip. For each measurement shown in Figure 2, we collected 10000 traces to generate 1D and 2D histograms without data selection.

III. Additional Figures and Tables

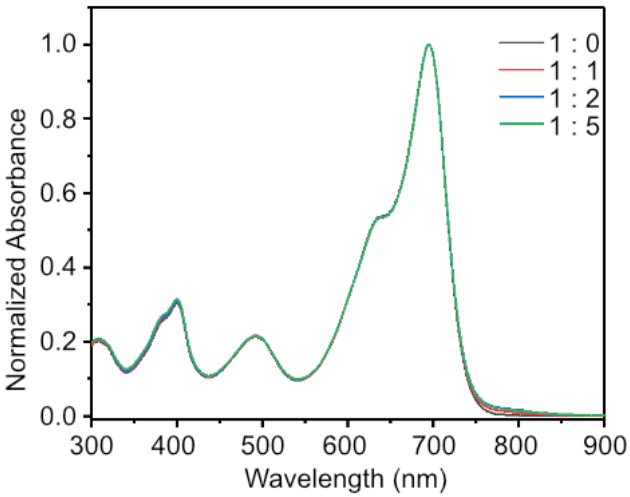

Figure S1. Normalized absorption spectra of 4 mM **1** (normalized at the peak ~ 697 nm) in deuterated chloroform with different amount of trifluoroacetic acid (TFA) added; the molar ratios between **1** and TFA are 1 : 0, 1 : 1, 1 : 2, and 1 : 5.

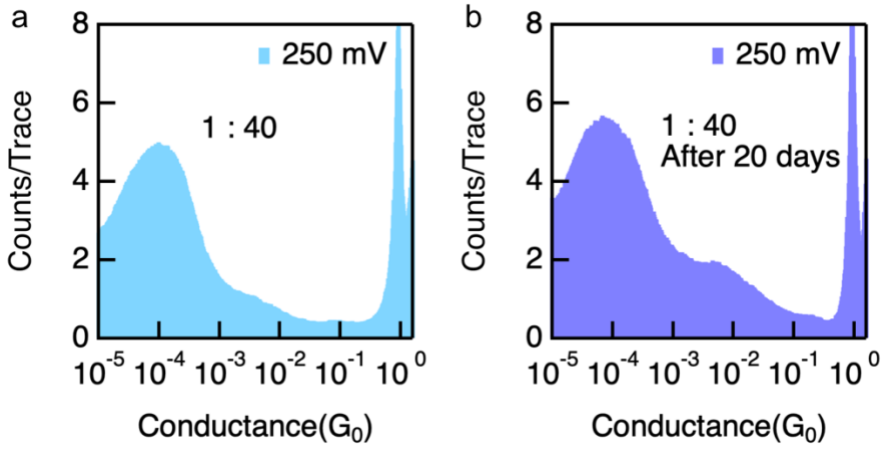

Figure S2. 1D histograms of **1** measured under molar ratio between **1** and TFA at 1 : 40 at 250 mV for (a) a fresh solution and (b) a molecular solution 20 days after it was prepared.

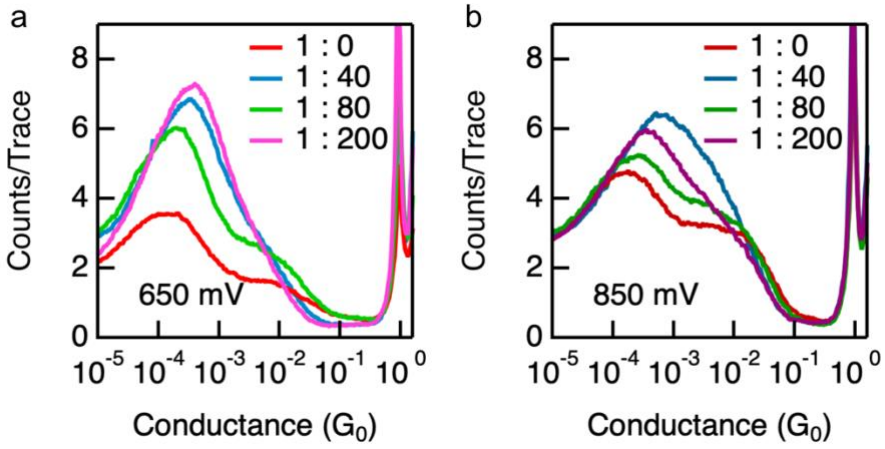

Figure S3. 1D histograms of **1** measured under molar ratio between **1** and TFA at 1 : 0, 1 : 40, 1 : 80, and 1 : 200 under (a) 650 mV and (b) 850 mV bias voltages. The histograms are reproduced from Figure 2 for an easy comparison of conductance histograms of **1** measured with different acid concentrations.

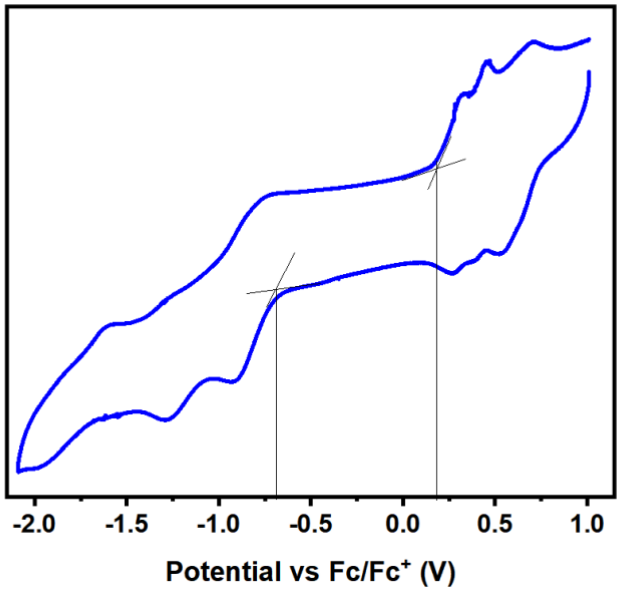

Figure S4. Cyclic voltammogram (CV) for compound **1** at 100 mV/s in dichloromethane containing 0.1M n-Bu_4NPF_6.

Notes for Figure S4

We use the following method for determining the electrochemical HOMO-LUMO gap.[4] The E_{HOMO} and E_{LUMO} are calculated according to equations (i) and (ii). The electrochemically determined band gaps are deduced from the difference between E_{LUMO} and E_{HOMO} based on equation (iii).

$$E_{HOMO} = -(E_{ox} + 4.8) \quad \text{(i)}$$

$$E_{LUMO} = -(E_{red} + 4.8) \quad \text{(ii)}$$

$$E_{g\_cv} = E_{LUMO} - E_{LUMO} \quad \text{(iii)}$$

As shown in Figure S4, oxidation and reduction potentials can be obtained by making tangent lines: E_{ox} = 0.18 eV and E_{red} = -0.69 eV. Thus E_{HOMO} = -(E_{ox}+4.8) = -4.98 eV, E_{LUMO} = -(E_{red}+4.8) = -4.11 eV, and $E_{g\_cv} = E_{LUMO} - E_{HOMO}$ = 0.87 eV.

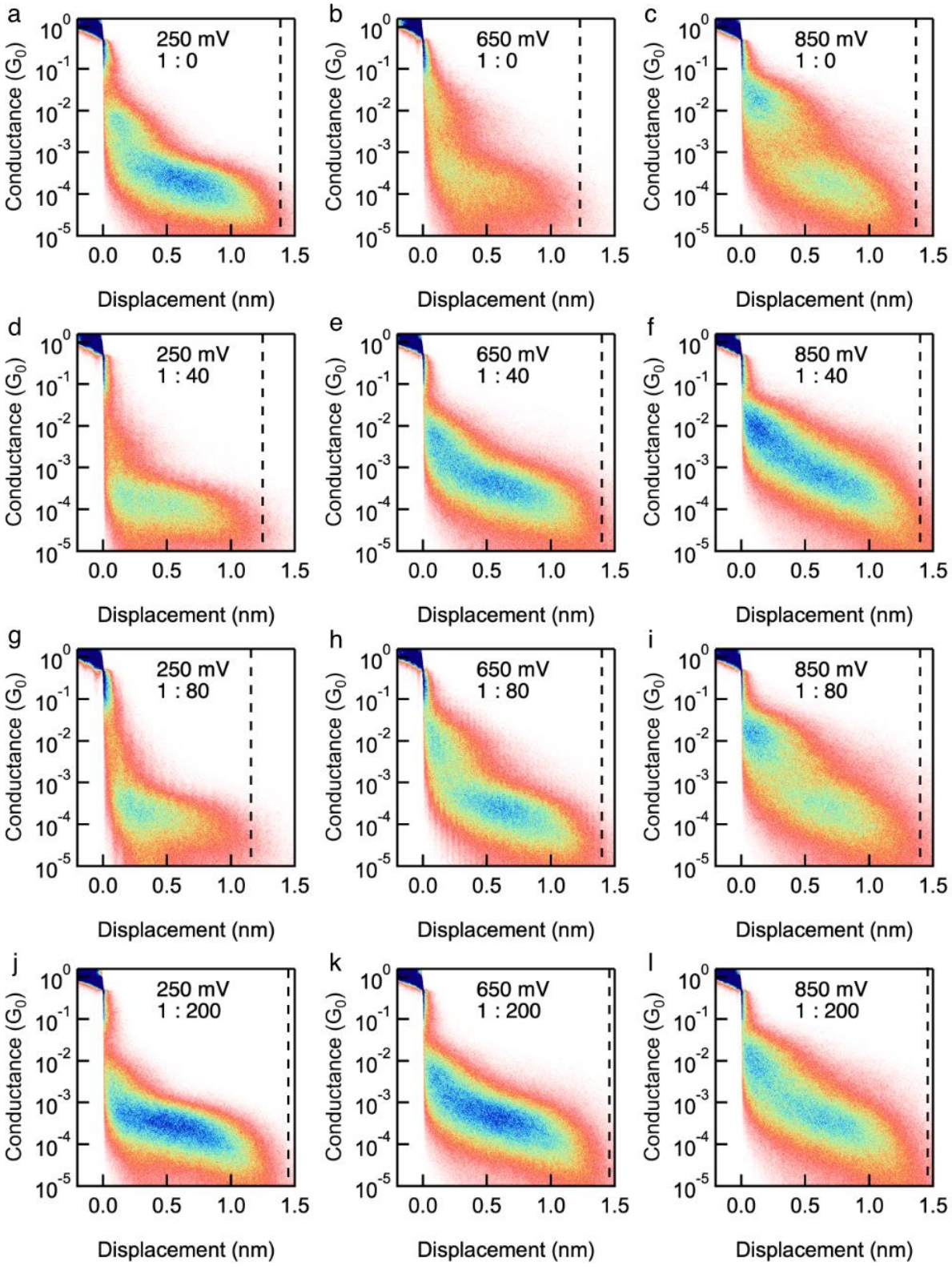
a
250 mV
1 : 0
b
650 mV
1 : 0
c
850 mV
1 : 0
d
250 mV
1 : 40
e
650 mV
1 : 40
f
850 mV
1 : 40
g
250 mV
1 : 80
h
650 mV
1 : 80
i
850 mV
1 : 80
j
250 mV
1 : 200
k
650 mV
1 : 200
l
850 mV
1 : 200
Conductance (G0)
Displacement (nm)

Figure S5. 2D histograms for **1** measured at molar ratio between **1** and TFA of (a-c) 1 : 0, (d-f) 1 : 40, (g-i) 1 : 80, and (j-l) 1 : 200 under 250 mV (left), 650 mV (middle), and 850 mV (right) tip bias voltages.

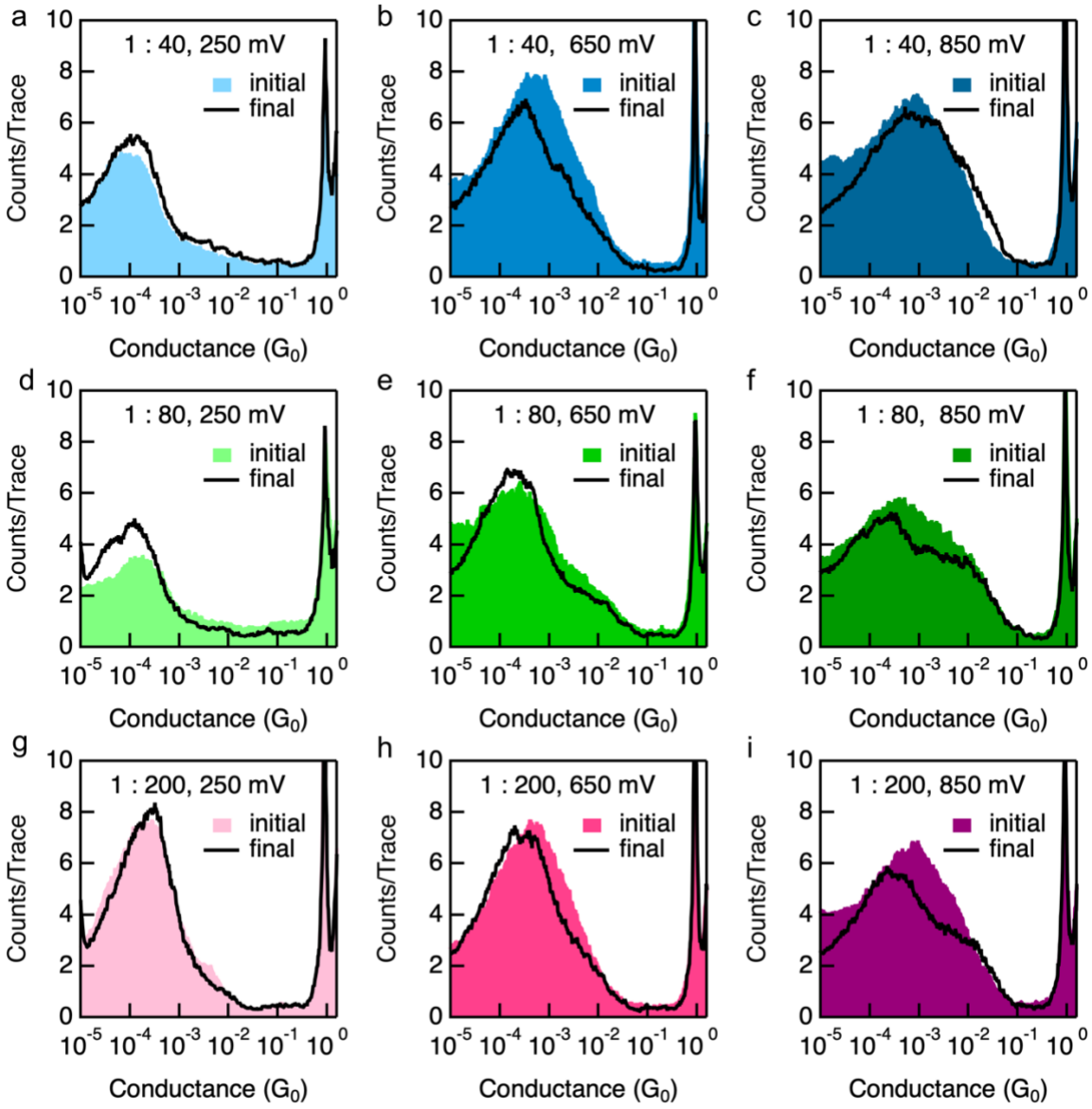

Figure S6. 1D histograms compiled from the first 1000 conductance traces (labeled as initial) and 9001-10000 conductance traces (labeled as final) in each experiment for **1** measured at molar ratio between **1** and TFA of (a-c) 1 : 40, (d-f) 1 : 80, and (g-i) 1 : 200 under 250 mV (left), 650 mV (middle), and 850 mV (right) tip bias voltages.

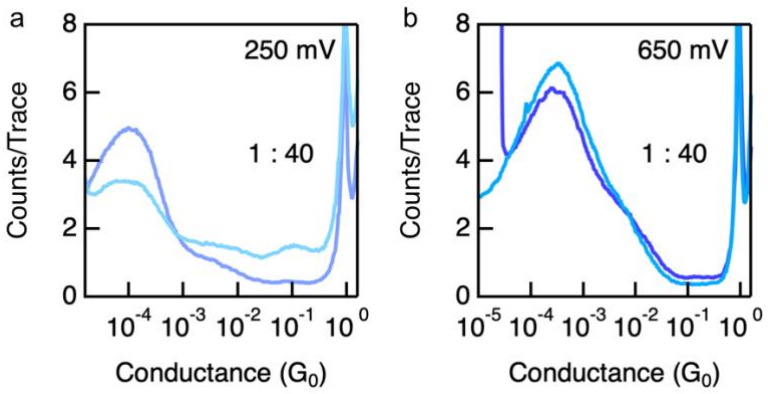

Figure S7. 1D conductance histograms of two repeated experiments of **1** performed on different days measured at molar ratio between **1** and TFA of 1 : 40 under (a) 250 mV and (b) 650 mV applied bias voltages.

Table S1. Measured conductances and junction elongation lengths for **1**.

Applied Voltage (mV)	Molar ratio of **1** : TFA	Conductance ($\times 10^{-4}$ G_0)	Junction elongation length (nm)[a]
250		1.7	1.39
650	1 : 0	1.3	1.23
850		1.6	1.37
250		0.97	1.25
650	1 : 40	3.0	1.40
850		6.9	1.40
250		1.2	1.16
650	1 : 80	1.3	1.40
850		2.4	1.40
250		2.2	1.45
650	1 : 200	3.5	1.46
850		3.6	1.46

[a]We determine the single-molecule junction elongation length as follows: we first integrate all counts in the 2D conductance histogram and create a 1D line profile along the displacement axis, then we use the displacement at which the intensity drops to 20% of its peak value as the junction elongation length.

IV. Computational Details

Structure optimizations: Molecular structures with thiomethyl (-SMe) terminated end groups were optimized within Kohn-Sham density functional theory (DFT) using the approximate exchange-correlation functional of Perdew-Burke-Enzerhof (PBE)[5] with Ahlrichs' def2-TZVP basis set,[6] while Grimme's DFT-D3[7] empirical dispersion corrections with Becke-Johnson damping[8] were considered. The longer end groups at

diazapentalenes were terminated using methyl groups before the optimization process. The atoms were relaxed until the change in total energy in the self-consistent-field algorithm reached below 10^{-7} a.u. and the gradient of the total energy with respect to nuclear displacements reached below 10^{-4} a.u. After optimization, single point energy calculations were done using B3LYP exchange correlation functional and def2-TZVP basis set to obtain the MOs plotted in Figure 4 in the main manuscript. All DFT calculations were performed using the TURBOMOLE V7.1 program package.[9]

Junction structures: To construct molecular junctions, both molecules were kept in between two fcc Au_{10} gold-clusters in such a way that the lone pairs on sulfur atoms in the -SMe end groups form donor-acceptor bonds with Au_{10} clusters' tip Au atoms. The Au-S distances were set to 2.30 Å as obtained from previous experimental studies.[10-11] The geometries are shown in Figure S8. The Au-Au bond lengths were kept at 2.88Å, which is the experimental value for bulk gold.[12]

Transmission function evaluation: For evaluating transmission functions, one-component scalar-relativistic single-point energy calculations were done on the junction structures (again with an SCF energy convergence threshold at 10^{-7} a.u.). For the single-point energy, one-component calculations were done with def2-TZVP basis set for all atoms with hybrid B3LYP exchange-correlation functional (in Figure 3 in the main manuscript). All of these calculations were performed using TURBOMOLE V7.1 program package.[9]

The effective single-particle Hamiltonian and overlap matrices were extracted using our postprocessing program package ARTAIOS.[13-14] We used the Landauer-Büttiker-Imry formalism[15] combined with Greens functions for the calculation of transmission functions,

$$T_{RL} = \mathrm{Tr}[\Gamma_L G_L \Gamma_R G_R^{\dagger}] \quad (1)$$

where

$$G = (ES_C - H_C - \Sigma_L - \Sigma_R)^{-1} \quad (2)$$

is the Green's function of the central region which contains only the molecule (without the gold clusters). E is the energy, H_C is the central-region part of the effective single-particle Hamiltonian expressed in an atom-centered basis (the Fock matrix), and S is the overlap matrix of the central region. The molecule-electrode coupling matrices are written as:

$$\Gamma_X = -2\,\mathrm{Im}\,\Sigma_X \quad (3)$$

where Σ_X are the self-energies of the left or right electrodes (X=R/L). Σ_X can be evaluated using the Hamiltonian and overlap matrices between central region and electrode region as:

$$\Sigma_X = (ES_{XC} - H_{XC})^{\dagger} g_X (ES_{XC} - H_{XC}) \quad (4)$$

where g_X is the Green's function of the electrode X, whose elements can be evaluated using a constant local density of states ($LDOS^{const.}$) as:

$$(g_x)_{ij} = -i\pi LDOS^{const.}\delta_{ij}. \quad (5)$$

Employing the wide-band limit, we set $LDOS^{const.}$ to 0.036 eV^{-1} as obtained from DFT for the 6s band of gold,[16-17] assuming a purely imaginary self-energy.

The MO energies are evaluated by solving secular equation of the central subsystem only using the equation:

$$H_C C_C = S_C C_C \varepsilon_C \quad (6)$$

where C_C and ε_C are the central subsystem MO coefficients and the subsystem matrix of Lagrangian Multipliers (MO energies), respectively. Identification of HOMO and LUMO were done by comparing their shapes of the MOs for the central subsystems and the isolated molecules. Where the MOs are close in energies, MO orders can change when going from isolated molecules to the junctions. In those cases, the HOMO and LUMO is assigned in such a way where the HOMO-LUMO gap is minimal. The subsystem MOs are shown in Figure S10.

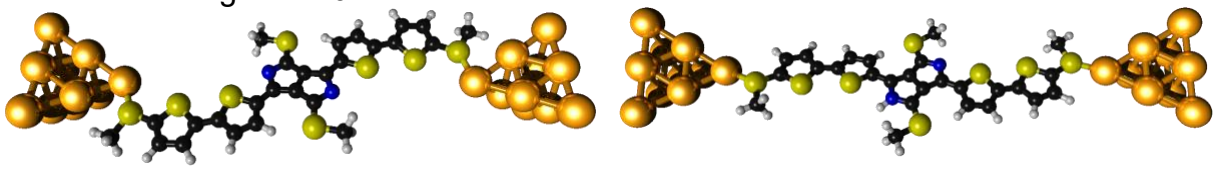

Figure S8. Junction geometries for **1** (left) and **1H** (right).

Calculation of peak width:
The peak width (*W*) were calculated using a formula:[18]
$W = 1.7 \times W_{1/2}$, Where $W_{1/2}$ is the full width at half maxima (FWHM). The approximate locations of those $W_{1/2}$ can be seen in Figure S12. The calculated *W* values for HOMO and LUMO levels for **1** are 0.37eV and 0.39 eV, whereas for **1H** those values are 0.46eV and 0.44eV. Therefore the HOMO level broadened by 0.09 eV and the LUMO level broadened by 0.05eV due to protonation.

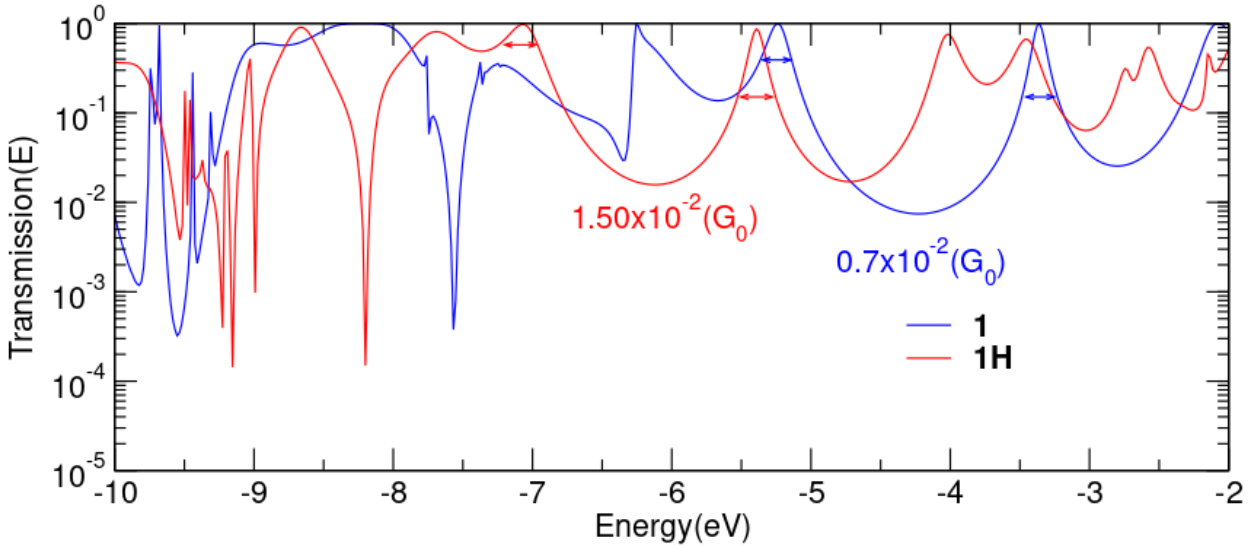

Figure S9. Comparison of transmission functions and location of FWHMs calculated with B3LYP functional and def2-TZVP basis set.

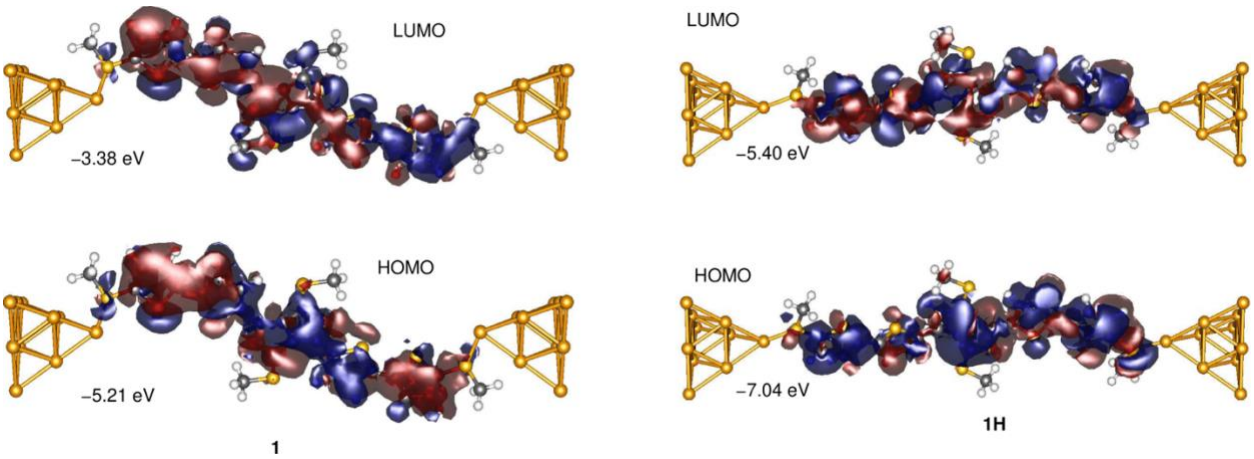

Figure S10. Subsystem MOs for **1** and **1H** from B3LYP exchange correlation functional and def2-TZVP basis set calculations.

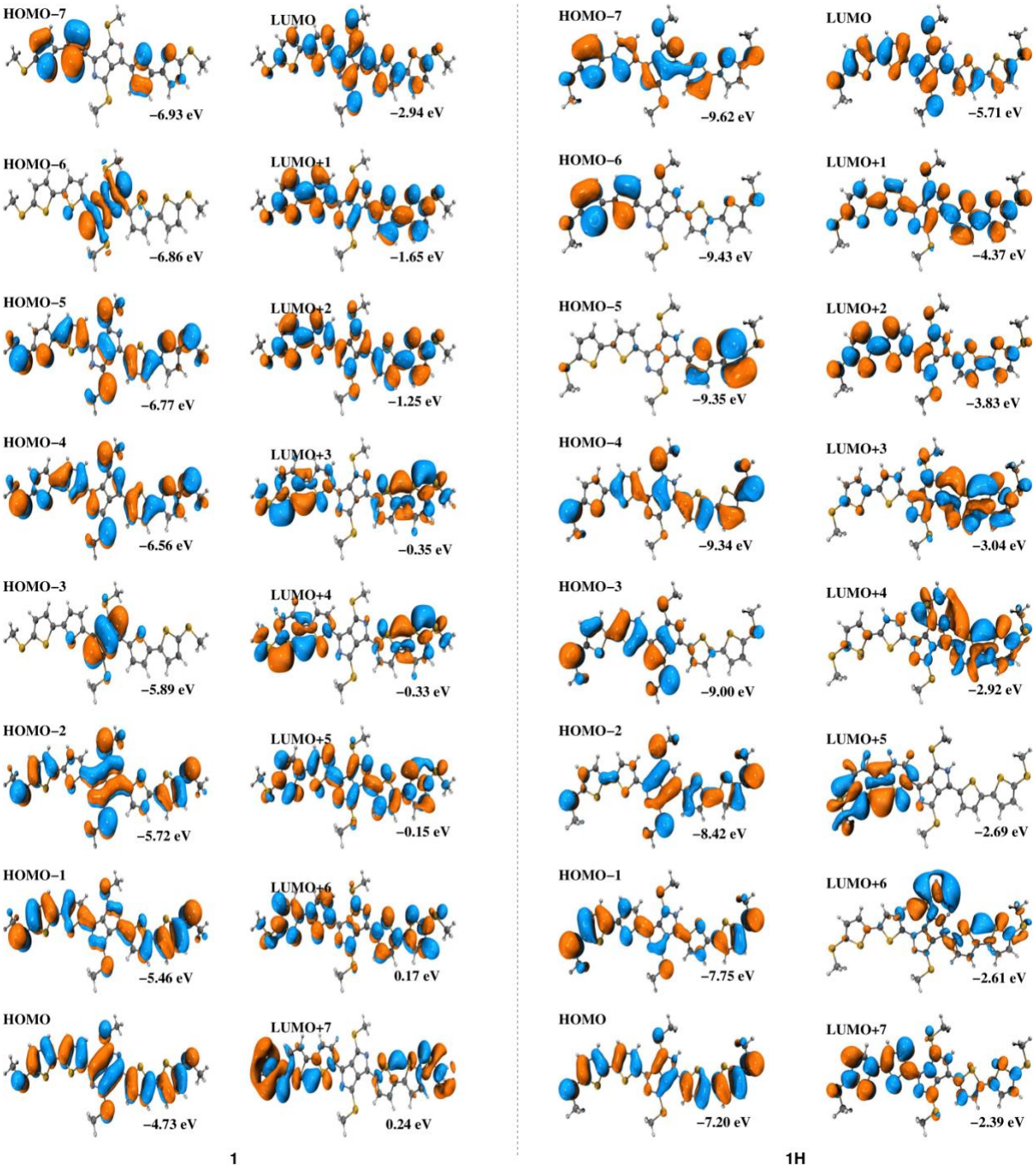

Figure S11: Frontier molecular orbitals for **1** and **1H** from B3LYP exchange correlation functional and def2-TZVP basis set calculations.

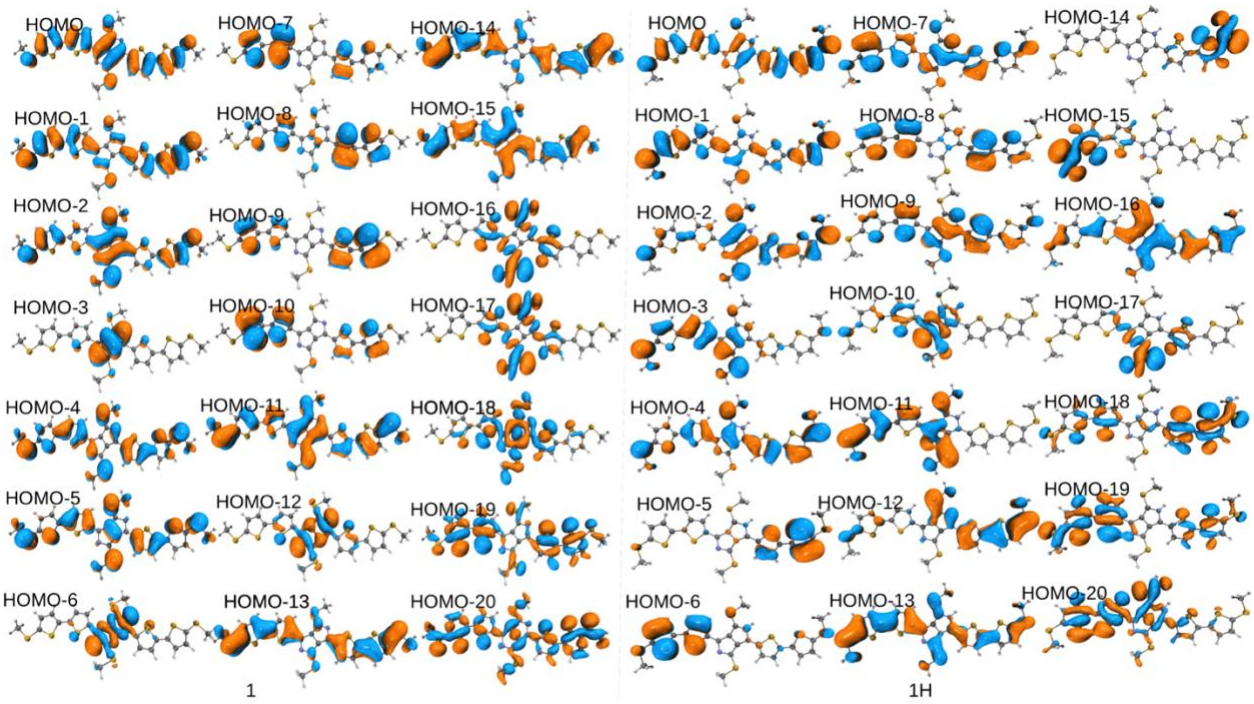

Figure S12. Lower energies occupied orbitals for **1** and **1H** from B3LYP exchange correlation functional and def2-TZVP basis set calculations.

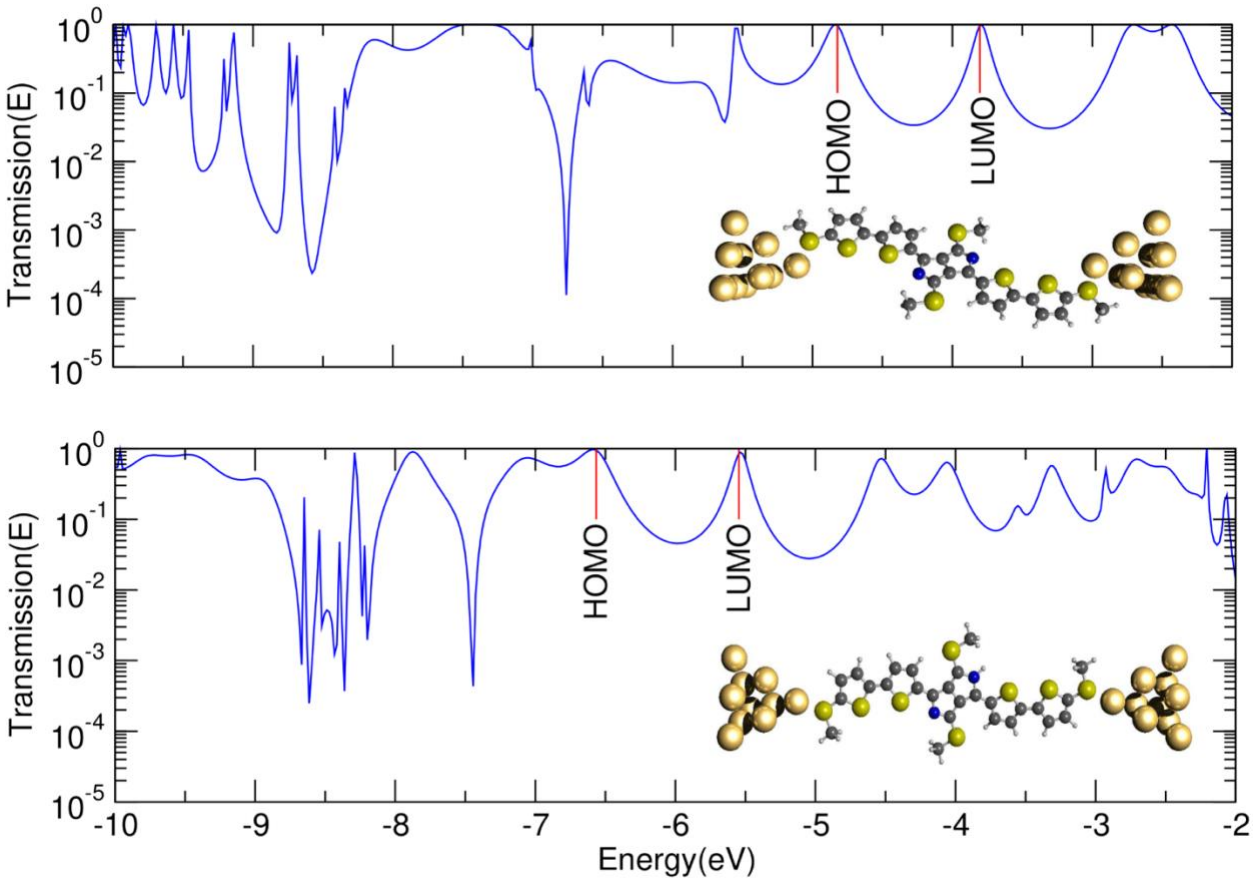

Figure S13: Transmission functions for **1** and **1H** junctions evaluated with PBE exchange correlation functional and def2-TZVP basis set.

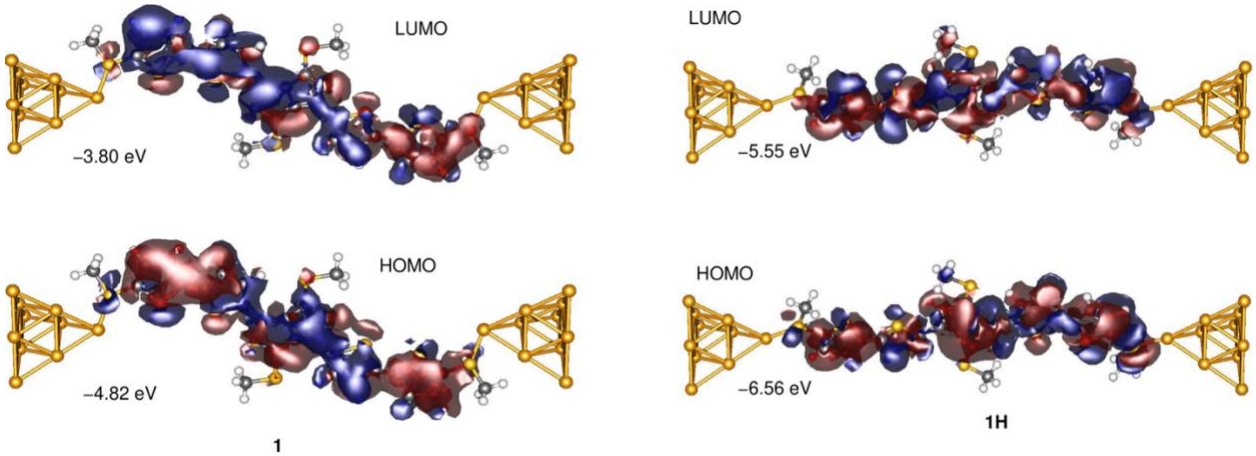

Figure S14. Subsystem MOs for **1** and **1H** from PBE exchange correlation functional and def2-TZVP basis set calculations.

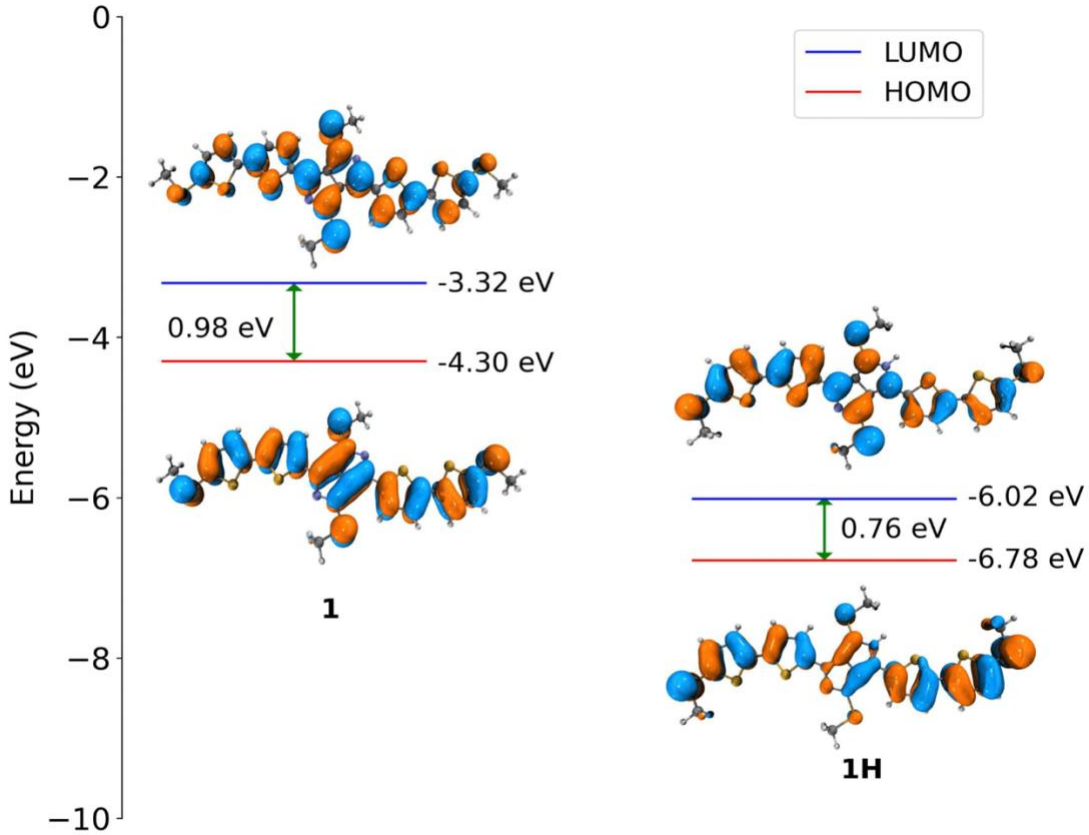

Figure S15: Energy level diagrams for HOMO and LUMO in both deprotonated **1** (left) and protonated **1H** (right) molecules with PBE exchange correlation functional and def2-TZVP basis set.

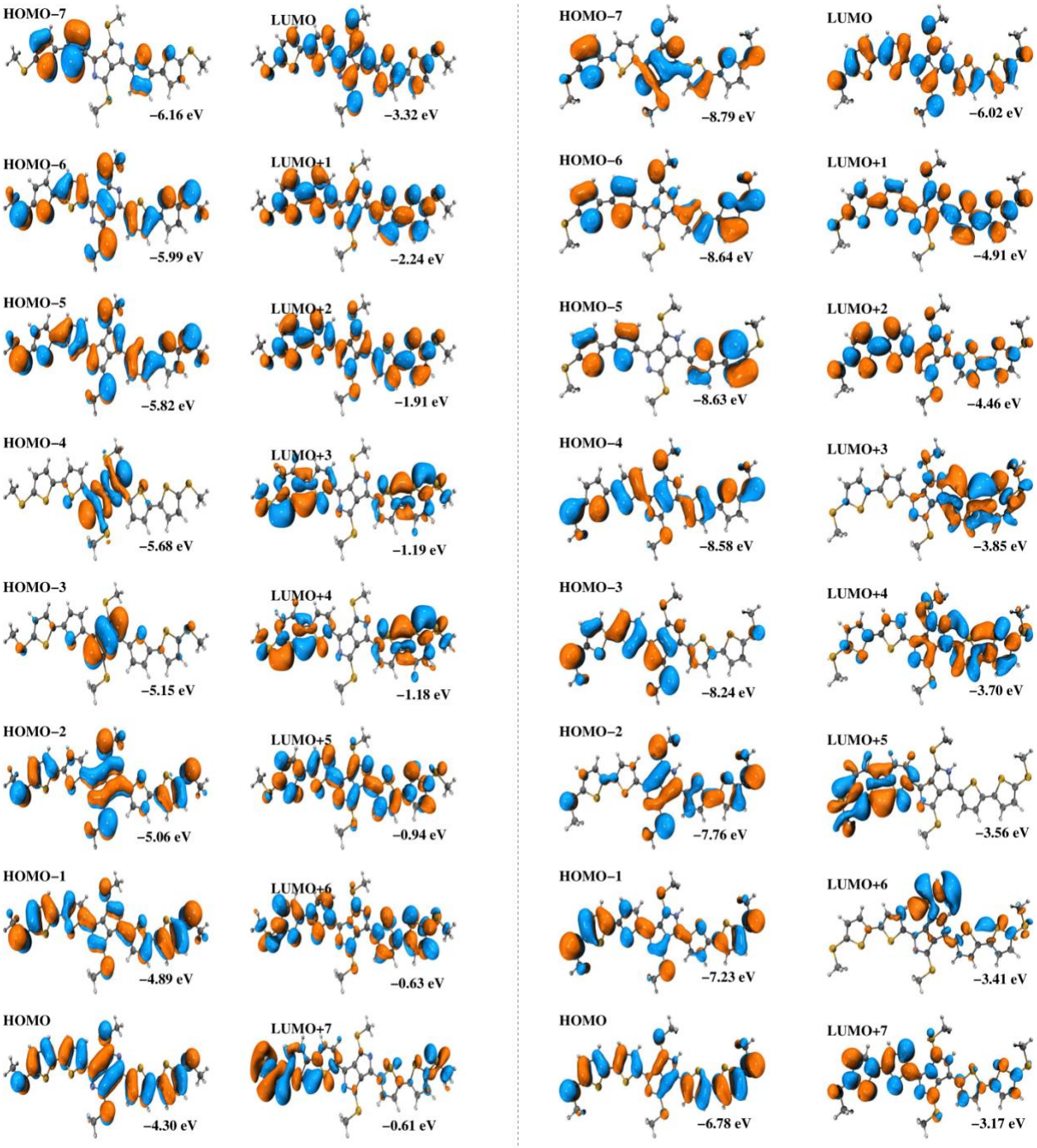

Figure S16. Frontier molecular orbitals for **1** and **1H** from PBE exchange correlation functional and def2-TZVP basis set calculations.

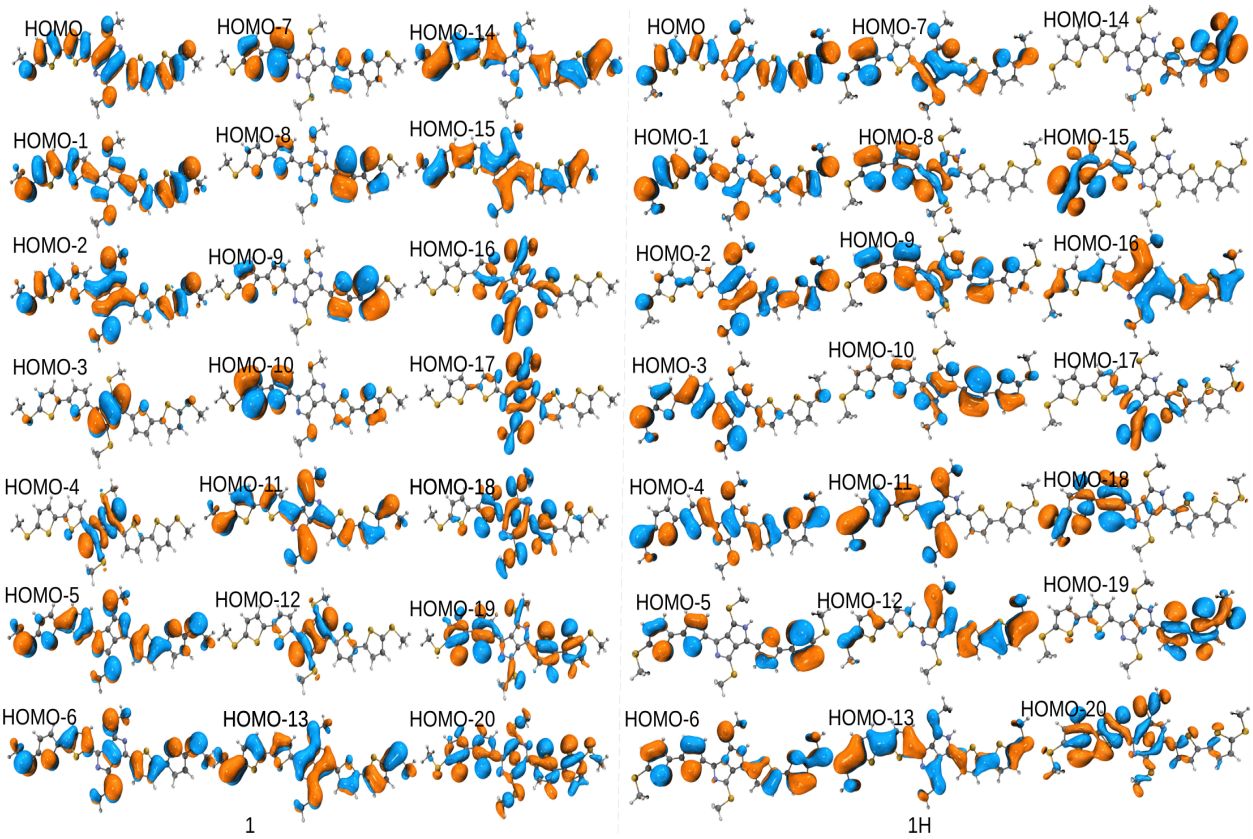

Figure S17. Lower energies occupied orbitals for **1** and **1H** from PBE exchange correlation functional and def2-TZVP basis set calculations.

Optimized geometries and dihedral angles: We checked the planarity of **1** and **1H** by calculating dihedral angle between the central diazapentalene and the thiophene rings. We found that they are almost the same in terms of planarity.

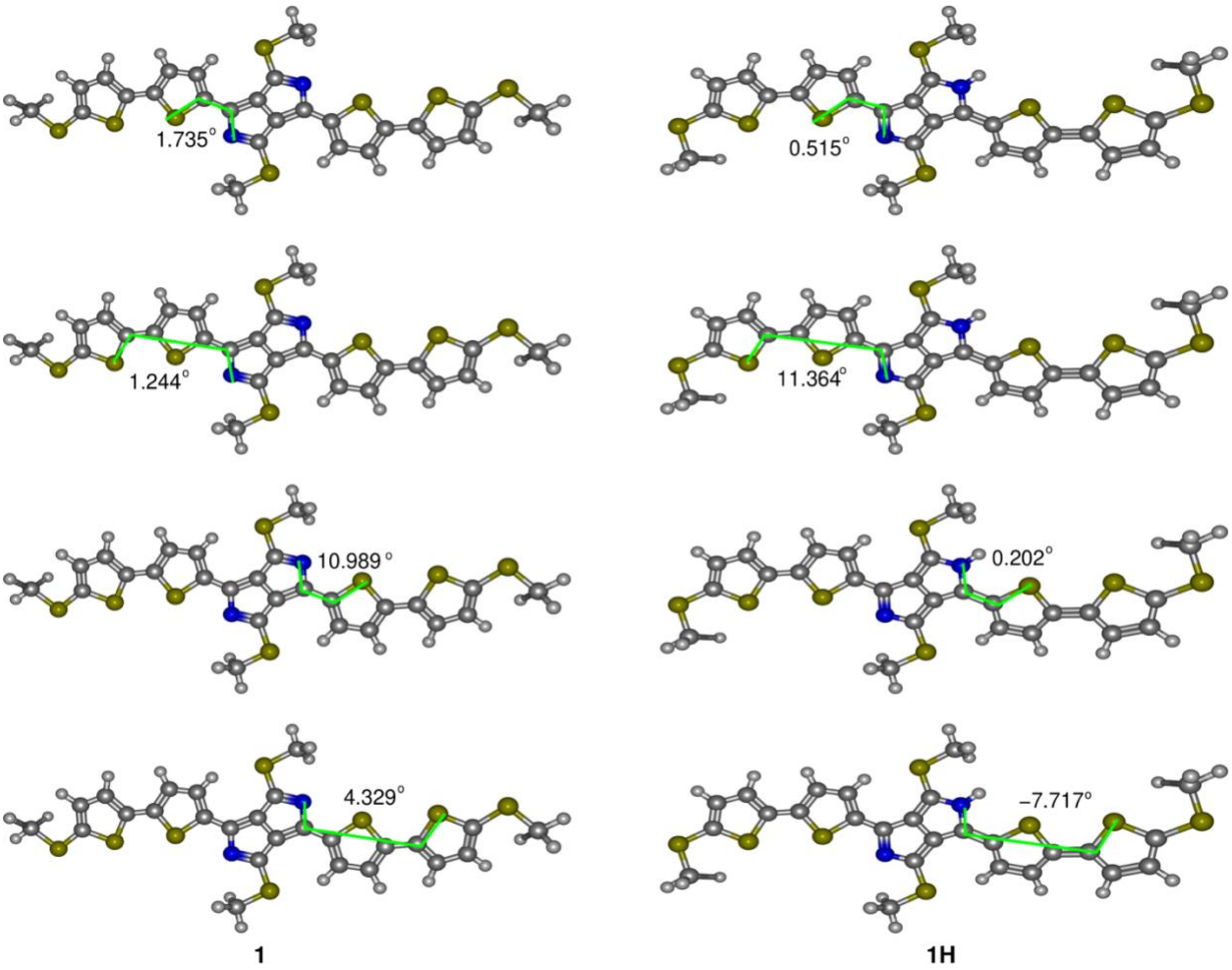

Figure S18. Optimized geometries and dihedral angles for **1** and **1H**.

Junction geometry for **1**.

C	-2.939811	-0.000000	17.686284
C	-4.173505	0.088200	18.315004
C	-4.099156	0.116030	19.725421
C	-2.797214	0.049039	20.196749
S	-1.664776	-0.056295	18.882856
H	-5.110728	0.145834	17.763406
H	-4.969517	0.188389	20.373764
C	-2.651531	-0.048107	16.281385
C	-3.566378	-0.182472	15.232169
S	-1.028482	0.061677	15.672115
C	-2.962081	-0.199730	13.969497
H	-4.638970	-0.279422	15.392518

C	-1.571633	-0.081553	14.018169
H	-3.510211	-0.301767	13.034614
C	-0.600741	-0.060505	12.981201
C	-0.730349	-0.151069	11.566781
C	0.590020	-0.075046	11.038124
C	1.440999	0.060917	12.184831
C	-1.581520	-0.281451	10.419732
C	0.460089	-0.163343	9.623476
N	-0.873784	-0.287628	9.273294
N	0.732824	0.068455	13.330704
C	1.435714	-0.145772	8.590752
C	2.827357	-0.049957	8.653391
S	0.906059	-0.267869	6.930396
C	3.443265	-0.065923	7.396578
H	3.368691	0.033207	9.594064
C	2.536719	-0.176416	6.337792
H	4.518298	0.019330	7.246168
C	2.843323	-0.213849	4.936337
C	4.080552	-0.366721	4.327427
S	1.597810	-0.044867	3.719907
C	4.031272	-0.357513	2.915804
H	5.000385	-0.502063	4.894486
C	2.745528	-0.196271	2.423502
H	4.907209	-0.473553	2.281444
S	-2.176544	0.053004	21.826260
S	2.159149	-0.125821	0.782461
S	-3.308019	-0.419239	10.428749
S	3.167103	0.205452	12.179575
C	3.507502	0.339759	13.951745
H	3.005110	1.221208	14.364890
H	3.154223	-0.557426	14.471611
H	4.596074	0.436404	14.044637
C	-3.654631	-0.545703	8.657078
H	-3.299970	0.352372	8.139543
H	-3.156669	-1.427468	8.239065
H	-4.743949	-0.638226	8.567542
C	-3.715745	0.110262	22.771575
H	-3.416216	0.102485	23.826655
H	-4.274049	1.031552	22.560807
H	-4.337041	-0.770631	22.563980
C	3.716541	-0.178971	-0.133821
H	3.440067	-0.106458	-1.192780
H	4.357581	0.670969	0.133744
H	4.244606	-1.126105	0.036620

Au	0.000000	-1.662740	27.270717
Au	-1.439970	0.831360	27.270717
Au	1.439970	0.831360	27.270717
Au	2.879940	-1.662740	27.270717
Au	-2.879940	-1.662740	27.270717
Au	-0.000000	3.325480	27.270717
Au	-1.439970	-0.831360	24.919247
Au	-0.000000	1.662740	24.919247
Au	1.439970	-0.831360	24.919247
Au	0.000000	-0.000000	22.567777
Au	0.000000	-1.662740	-4.702940
Au	1.439970	0.831360	-4.702940
Au	-1.439970	0.831360	-4.702940
Au	-2.879940	-1.662740	-4.702940
Au	2.879940	-1.662740	-4.702940
Au	0.000000	3.325480	-4.702940
Au	1.439970	-0.831360	-2.351470
Au	0.000000	1.662740	-2.351470
Au	-1.439970	-0.831360	-2.351470
Au	0.000000	0.000000	0.000000

Junction geometry for **1H**.

C	-1.120543	-0.000000	5.969472
C	-2.000039	-0.492772	5.000803
C	-1.519582	-0.387205	3.692118
C	-0.250975	0.193841	3.625838
S	0.332245	0.605218	5.205867
H	-2.969708	-0.920372	5.250234
H	-2.061768	-0.718337	2.807986
C	-1.302430	0.035232	7.379469
C	-2.427162	-0.421847	8.095798
S	-0.101677	0.675106	8.459335
C	-2.306712	-0.256974	9.469163
H	-3.298155	-0.858015	7.610929
C	-1.091522	0.329267	9.861194
H	-3.078995	-0.547058	10.178677
C	-0.592889	0.647147	11.138302
C	-1.145388	0.437056	12.454372
C	-0.172186	0.949001	13.378584
C	0.904473	1.430679	12.554627
C	-2.187857	-0.112261	13.207963
C	-0.621310	0.709515	14.687308

N	-1.848645	0.051723	14.535073
N	0.638585	1.251717	11.248541
C	-0.084091	0.975746	15.972318
C	0.999609	1.788433	16.316609
S	-0.769629	0.257526	17.415247
C	1.249377	1.840866	17.688768
H	1.568010	2.350934	15.578560
C	0.369211	1.067219	18.455658
H	2.041887	2.438266	18.134952
C	0.357599	0.901902	19.872434
C	1.284047	1.385923	20.796604
S	-0.904111	0.018276	20.698227
C	0.985752	1.055630	22.125337
H	2.162426	1.959361	20.504817
C	-0.181461	0.304424	22.249871
H	1.592070	1.346969	22.981378
S	0.626230	0.468663	2.162912
S	-0.831185	-0.269603	23.748163
S	-3.649983	-0.868298	12.677514
C	-4.402192	-1.410616	14.232343
H	-3.743516	-2.104052	14.770858
H	-4.689037	-0.556037	14.859509
S	2.368007	2.147720	13.112736
C	3.220121	2.481330	11.553220
H	3.393860	1.545148	11.012232
H	2.621691	3.162488	10.938914
H	-2.474414	-0.142117	15.309896
H	4.172563	2.948719	11.829909
H	-5.313479	-1.946000	13.940193
C	2.160016	1.217160	2.759355
H	2.762287	1.409453	1.863389
H	1.959255	2.167237	3.271553
H	2.701916	0.526487	3.418595
C	-2.327789	-1.134419	23.218810
H	-2.782531	-1.526229	24.136602
H	-3.029484	-0.443677	22.733617
H	-2.082415	-1.971550	22.552176
Au	0.000000	-1.662740	30.578648
Au	-1.439970	0.831360	30.578648
Au	1.439970	0.831360	30.578648
Au	2.879940	-1.662740	30.578648
Au	-2.879940	-1.662740	30.578648
Au	-0.000000	3.325480	30.578648
Au	-1.439970	-0.831360	28.227178

Au	-0.000000	1.662740	28.227178
Au	1.439970	-0.831360	28.227178
Au	0.000000	-0.000000	25.875708
Au	0.000000	-1.662740	-4.702940
Au	1.439970	0.831360	-4.702940
Au	-1.439970	0.831360	-4.702940
Au	-2.879940	-1.662740	-4.702940
Au	2.879940	-1.662740	-4.702940
Au	0.000000	3.325480	-4.702940
Au	1.439970	-0.831360	-2.351470
Au	0.000000	1.662740	-2.351470
Au	-1.439970	-0.831360	-2.351470
Au	0.000000	0.000000	0.000000

V. NMR spectra

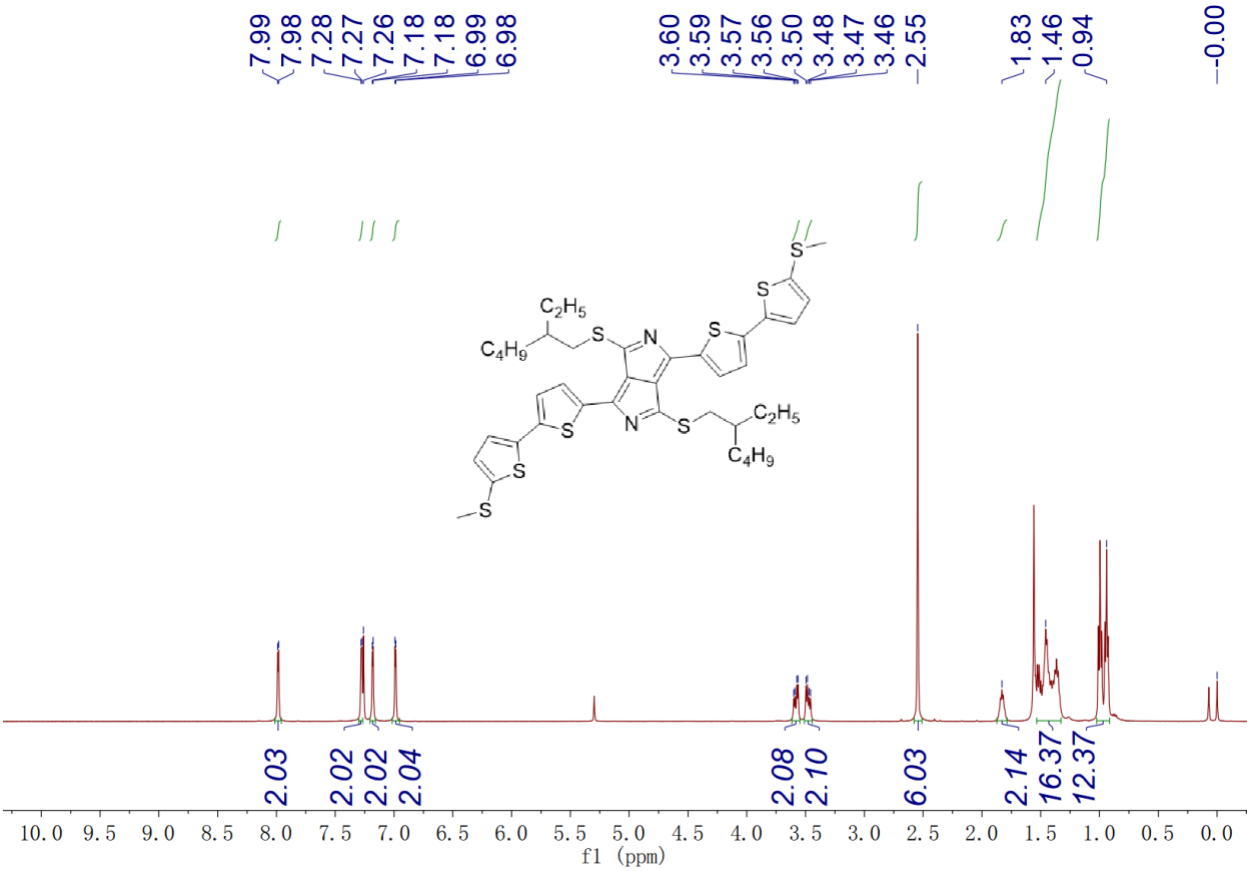

Figure S19. ^{1}H NMR spectra for **1**.

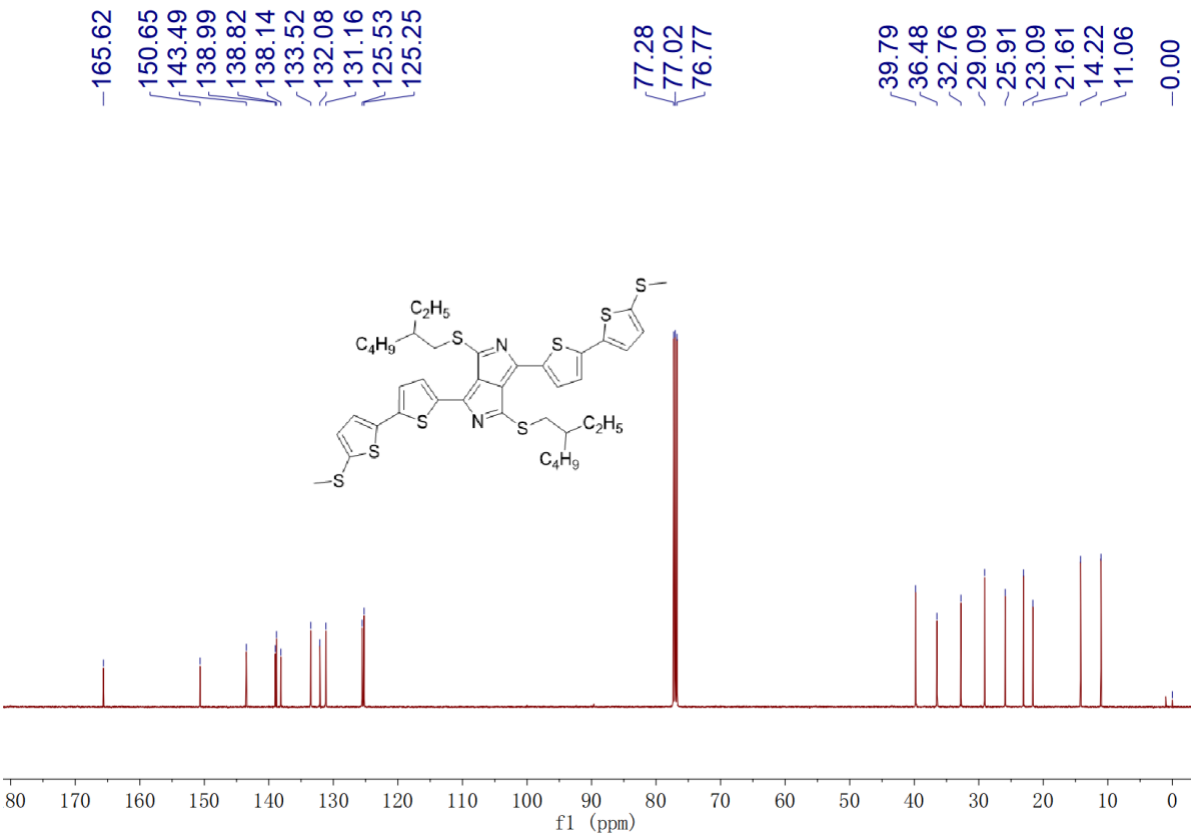

Figure S20. ^{13}C NMR spectra for **1**.

VI. Mass spectrum

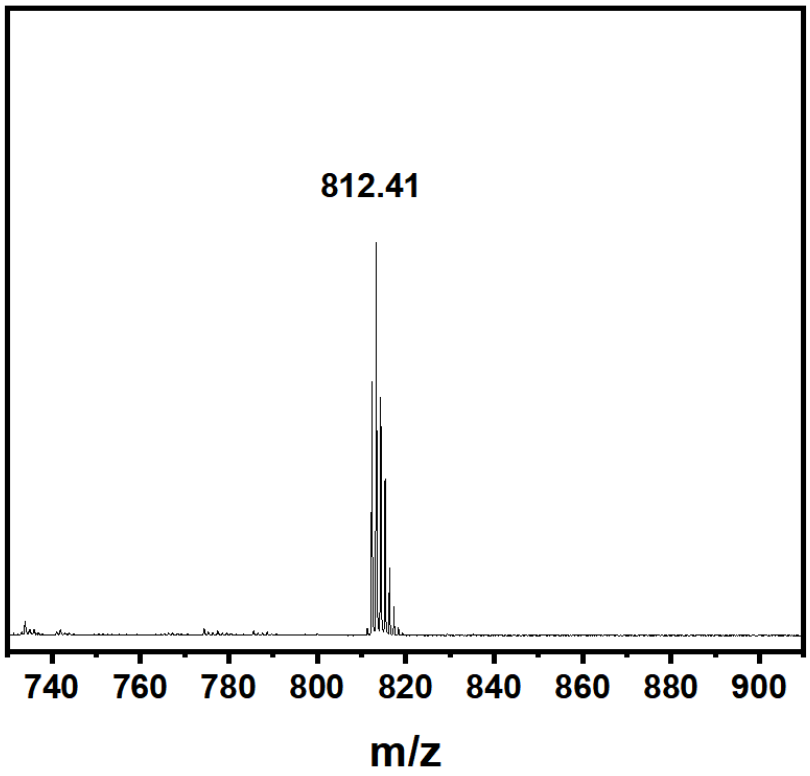

Figure S21. MALDI-TOF mass spectrum for **1**.

VII. References

1. Qian, G.; Wang, Z. Y., Near-Infrared Thermochromic Diazapentalene Dyes. *Advanced Materials* **2012,** *24* (12), 1582-1588.
2. Dell, E. J.; Capozzi, B.; Xia, J.; Venkataraman, L.; Campos, L. M., Molecular length dictates the nature of charge carriers in single-molecule junctions of oxidized oligothiophenes. *Nature Chemistry* **2015,** *7* (3), 209-214.
3. Guo, W.; Quainoo, T.; Liu, Z.-F.; Li, H., Robust binding between secondary amines and Au electrodes. *Chemical Communications* **2024**.
4. Hu, L.; Wu, F.; Li, C.; Hu, A.; Hu, X.; Zhang, Y.; Chen, L.; Chen, Y., Alcohol-Soluble n-Type Conjugated Polyelectrolyte as Electron Transport Layer for Polymer Solar Cells. *Macromolecules* **2015,** *48* (16), 5578-5586.
5. Perdew, J. P.; Burke, K.; Ernzerhof, M., Generalized Gradient Approximation Made Simple. *Physical Review Letters* **1996,** *77* (18), 3865-3868.
6. Weigend, F.; Ahlrichs, R., Balanced basis sets of split valence, triple zeta valence and quadruple zeta valence quality for H to Rn: Design and assessment of accuracy. *Physical Chemistry Chemical Physics* **2005,** *7* (18), 3297-3305.

7. Grimme, S.; Antony, J.; Ehrlich, S.; Krieg, H., A consistent and accurate ab initio parametrization of density functional dispersion correction (DFT-D) for the 94 elements H-Pu. *The Journal of Chemical Physics* **2010,** *132* (15).
8. Grimme, S.; Ehrlich, S.; Goerigk, L., Effect of the damping function in dispersion corrected density functional theory. *Journal of Computational Chemistry* **2011,** *32* (7), 1456-1465.
9. TURBOMOLE V7.1 2016, a development of University of Karlsruhe and Forchungszentrum Karlsruhe GmbH, 1989-2007, TURBOMOLE GmbH since 2007; available from https://www.turbomole.com.
10. Bürgi, T., Properties of the gold–sulphur interface: from self-assembled monolayers to clusters. *Nanoscale* **2015,** *7* (38), 15553-15567.
11. Qian, H.; Eckenhoff, W. T.; Zhu, Y.; Pintauer, T.; Jin, R., Total Structure Determination of Thiolate-Protected Au38 Nanoparticles. *Journal of the American Chemical Society* **2010,** *132* (24), 8280-8281.
12. Fishman, J.; Yarish, M., Gold-palladium electrocatalysts. *Electrochimica Acta* **1967,** *12* (5), 579-581.
13. Herrmann, M. D. L. G. T. S. B. A. V. G. C. S. C., ARTAIOS- a transport code for postprocessing quantum chemical electronic structure calculations, available from https://www.chemie-uni-hamburg.de/ac/herrmann/software/index.html.
14. Herrmann, C.; Solomon, G. C.; Subotnik, J. E.; Mujica, V.; Ratner, M. A., Ghost transmission: How large basis sets can make electron transport calculations worse. *The Journal of Chemical Physics* **2010,** *132* (2).
15. Landauer, R., Spatial variation of currents and fields due to localized scatterers in metallic conduction. *IBM Journal of research and development* **1957,** *1* (3), 223-231.
16. Papaconstantopoulos, D., Handbook of the band structure of elemental solids. Plenum Press. *New York* **1986**.
17. Chen, Y.; Prociuk, A.; Perrine, T.; Dunietz, B. D., Spin-dependent electronic transport through a porphyrin ring ligating an Fe (II) atom: An ab initio study. *Physical Review B—Condensed Matter and Materials Physics* **2006,** *74* (24), 245320.
18. Gjerde, D. T.; Hoang, L.; Hornby, D., *RNA purification and analysis: sample preparation, extraction, chromatography*. John Wiley & Sons: 2009.